An investigation of electrowetting-based microactuation

Ed Colgate and Hirofumi Matsumoto
Department of Mechanical Engineering, Northwestern University, Evanston, Illinois 60208

(Received 22 August 1989; accepted 15 January 1990)

Electrical control of the interfacial tension between a liquid and solid ("electrowetting") has been studied as a means of actuation in the microdomain (characteristic dimensions 1 μm–1 mm). Electrowetting provides a means of direct fluid pumping with no moving mechanical parts, which may prove useful in a number of application areas, most notably the liquid cooling of high-density microelectronic devices. A detailed model of a test device for the study of electrowetting is presented. The model describes liquid flow in a small channel, as governed as the Navier–Stokes equations, Young's equation, and Lippmann's equation (for the effect of an applied potential on interfacial tension). Simulation results are presented. Preliminary results indicate that electrowetting is a viable approach to microactuation: in a 10 μm radius channel, it may be used to generate pressures on the order of 0.01 MPa, comparable to pressures generated by existing micropump designs, which are orders of magnitude larger in size.

I. INTRODUCTION

A. Microelectro mechanical systems

In the last several years, fueled largely by novel applications of silicon processing techniques, a small number of researchers have begun to develop a variety of microscopic mechanical components, including pin joints, gears, springs, levers, and most recently, electric motors. To many, such components hold the promise of a revolution of miniaturization that will change the discipline of mechanical engineering as profoundly as the microelectronics revolution changed electrical engineering. Before this can occur, however, it will be necessary to develop means of interconnecting these components, as well as actuators, sensors, and computational components, into microelectro mechanical systems (MEMS). Thus, research topics of basic importance include the development of a useful catalog of actuators, and means of integrating these actuators into mechanical systems. The subject of this paper is actuation for fluid microsystems; i.e., *micropumping*.

A variety of applications for fluid microsystems have been suggested, including electronic fuel injectors for automobiles, miniature chemical dispensers and reactors, miniature blood analyzers, and high performance heat sinks for high-density microelectronic devices. The last of these is of particular interest, because it has been demonstrated that "microchannel cooling" can effectively dissipate up to 790 W/cm^2, approximately 40 times greater than that achieved with conventional heat sinks.[1] The microchannel heat sink for these experiments consisted of water flowing through an array of parallel channels, each 300 μm high and 50 μm wide, at rates of up to 8.6 cm^3/s.

Where pumping is required in such applications, there are certainly many instances in which a conventional, macrosized pump would suffice. For instance, the microchannel heat sink was designed so that all of the channels communicated with common manifolds at their ends. These manifolds were easily plumbed into an ordinary supply. However, there are reasons that a micropump, or collection of micropumps, might be an attractive or even necessary alternative. For instance, micropumps are essential if self-contained microsystems are to be developed. Transmission losses, as well as inlet and outlet losses, which can be significant in fluid microsystems, would be minimized by using integrated pumps. Distributed pumping is expected to be important in a number of instances because the total pressure drop across a fluid microsystem is liable to be quite large. High pressures are demanding of the pump, and may even, in the case of microchannel cooling, cause the silicon substrate to warp.[2] A better approach may well be distributed micropumping with each pump responsible for only a fraction of the total load, or even arrays of independent fluid microsystems, each with its own pump. In instances when dynamics are important, local pumping should keep fluid inertia and fluid resistance to a minimum, improving response times. Finally, if there are many different flows to be controlled, it may be simpler and more energy efficient to employ multiple pumps than multiple adjusting valves.

B. Micropump designs

The first working micropumps to have been developed employ piezoelectric actuation of silicon membranes.[3,4] Selected characteristics of these pumps are listed in Table I. It can be seen that neither pump achieves microscopic dimensions. This is in large part due to the space required for the silicon membranes. The pumping mechanism described in this paper is distinct in that it will lead to pump designs that

TABLE I. Comparison of existing micropump designs.

Pump	Ref. 3	Ref. 4
Test medium	water	nitrogen gas
Max flow rate (μl/s)	0.8	0.333
Max pressure (MPa)	0.01	0.008
Means of actuation	piezo disc/glass membrane	piezo stack/silicon membrane
Membrane width (mm)	12.5	4.0
Membrane thickness (μm)	300	50
Max height (mm above wafer)	0.11	9.0

 0734-2101/90/043625-09$01.00

are truly microscopic; indeed, the physical phenomenon on which this mechanism is based, surface tension, becomes important only when characteristic dimensions drop well below 1 mm.

II. SURFACE TENSION

A. Surface and interfacial tensions

As is well-known, energy is required to increase the surface area of any liquid, and this energy per unit surface area is the liquid's surface tension, γ. Surface tension is a manifestation of the imbalance of intermolecular (van der Waals) forces acting on molecules at a surface. van der Waals forces arise due to dipole/dipole interactions (in polar liquids), London dispersion forces (fluctuating induced dipoles), metallic bonds (in liquid metals), and hydrogen bonds. Intermolecular forces occur in gases as well; however, because the forces decrease rapidly as a function of intermolecular distance, they are essentially negligible for most gases. Solids also experience surface tension, which may be affected by other intermolecular forces, such as covalent bonding.

When two phases come into contact, an interfacial tension is set up that is the sum of the two surface tensions, less an energy lowering associated with attractive forces between the molecules of the two phases. In many cases, the interfacial tension can be approximated as[5]

$$\gamma_{12} = \gamma_1 + \gamma_2 - 2\sqrt{\gamma_1^d \gamma_2^d}, \tag{1}$$

where γ_1^d is the component of γ_1 due to London dispersion forces (the dominant component of surface tension in most liquids), and likewise for γ_2^d.

When liquid is in contact with both a solid and a gas, as shown in Fig. 1(a), a "contact angle" of between 0° and 180° is set up. Young's equation, which is essentially a horizontal force balance applied to the interface, describes the static relation of the three interfacial tensions:

$$\gamma_{SL} + \gamma_{LG} \cos\theta = \gamma_{SG}, \tag{2}$$

where θ is the contact angle. In the example shown in Fig. 1(a), for instance, $\cos\theta$ is positive, indicating that the solid–liquid interface is of lower energy that the solid–gas interface. In such a case, we can also expect to see the phenomenon of capillary rise, illustrated in Fig. 1(b). In order to seek a lower interfacial energy state, liquid will rise up the capillary. If the liquid rises a distance l, the energy reduction is $(\gamma_{SG} - \gamma_{SL})2\pi al$, where a is the capillary radius. Work, however, will also be done to raise the column of liquid; this work will be $\Delta P \pi a^2 l$, where ΔP is the (constant) pressure difference between the top and bottom of the column. Equating these energies, and using Eq. (2), we have:

$$\Delta P = \frac{2(\gamma_{SG} - \gamma_{SL})}{a} = \frac{2\gamma_L \cos\theta}{a}, \tag{3}$$

where we have also made use of the fact that, generally, $\gamma_L \approx \gamma_{LG}$. Equation (3), which indicates the pressure drop across a liquid–gas interface in a small capillary, is of basic importance in the sequel.

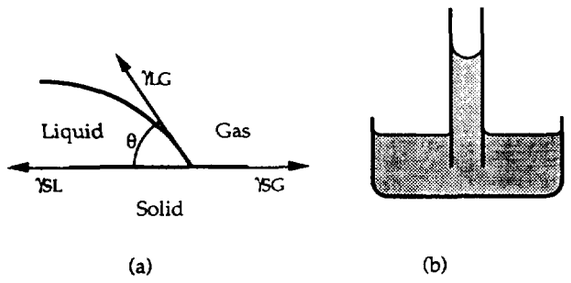

FIG. 1. (a) A liquid in contact with both a gas and a solid. Static equilibrium requires that the horizontal components of the interfacial tensions sum to zero, as expressed in Young's equation. (b) Capillary rise, the liquid–gas interface in the capillary supports a pressure discontinuity.

B. Electrical control of surface tension

Consider the interface between a conducting solid and an electrolytic fluid. When an electric potential is applied across this interface, a layer of charge builds up on the surface of the solid, and were it not for diffusive processes, a layer of charge of opposite sign would build up on the surface of the liquid. In such a case, the change in potential would be very abrupt, occurring over distances on the order of a single molecular diameter. In reality, the charge distribution in the liquid will be somewhat diffuse, and the change in potential somewhat less abrupt, although it will still occur over distances typically on the order of a few angstroms.

In the late 19th century, Helmholtz proposed a model for the electric "double layer" as a parallel plate capacitor, with the metal surface as one plate, and an imaginary layer of charge in the liquid as the other plate (Fig. 2). The distance between the plates would equal the approximate width of the diffuse "interphase" region in the liquid, over which the electric field drops to near zero. This model, although it has been refined since, appears to be essentially correct.[6] Assuming that the width of the double layer is small compared to the curvature of the surface, its capacitance per unit area will be:

$$C/A = \frac{\epsilon_r \epsilon_0}{\delta}, \tag{4}$$

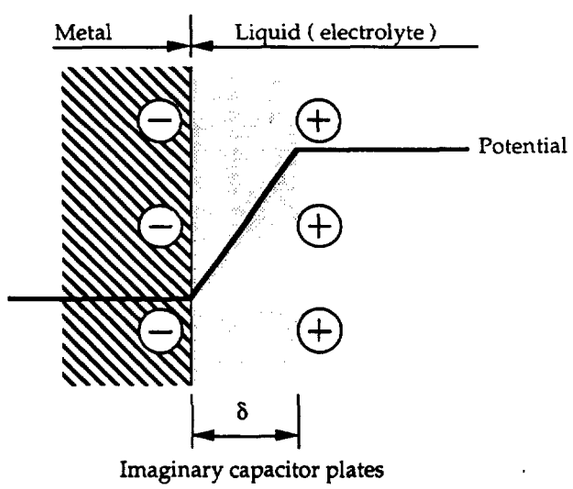

FIG. 2. Helmoltz model of the electric double layer. Although the charge distribution in the liquid is actually diffuse, it is modeled as a sheet of charge a distance δ from the metal surface.

where ϵ_0 is the permittivity of free space, ϵ_r is the relative permittivity of the electrolyte, and δ is the thickness of the double layer. It is worth noting that, because δ may be quite small, the capacitance of the double layer may be quite large—on the order of $10\,\mu F/cm^2$. Given an applied potential V, the energy per unit area stored in the double layer is:

$$U/A = \frac{\epsilon_r \epsilon_0}{2\delta} V^2. \tag{5}$$

Making the approximation that this energy is stored in the interface rather than the interphase, the total energy per unit area required to create new surface is:

$$\gamma_{SL} = \gamma_{SL}^{max} - \frac{\epsilon_r \epsilon_0}{2\delta}(V - V^{zc})^2, \tag{6}$$

where V^{zc} is the potential of zero charge for the electrolyte (typically not zero), and γ_{SL}^{max} is the surface tension corresponding to $V = V^{zc}$, and therefore to the absence of charge in the double layer. Equation (6), an integral version of Lippman's equation, indicates how an applied voltage may alter the apparent surface tension at the solid–liquid interface, the phenomenon known as electrowetting.[7]

III. A TEST DEVICE FOR ELECTROWETTING-BASED MICROACTUATION

A. Description of the test device

A simple device for the study of electrowetting is under construction, and is illustrated in Fig. 3. The device consists of a set of channels of varying widths (3–400 μm) connected to a common reservoir. The channels and reservoir are etched into a silicon wafer to a depth of 12 μm, with reactive ion etching. A layer of NiCr, which serves as one electrode, is deposited on the channels. A second electrode is deposited on top of an insulating layer of SiO_2 in the reservoir. The channels are covered with a glass plate (anodically bonded to the NiCr),[8] which permits viewing of the liquid–gas interface within. The reservoir can be filled with a pipette. Liquid will be drawn into the capillaries, assuming a contact angle of less than 90°. A voltage applied via probe tips across the two electrodes will alter the solid–liquid interfacial tension, and will cause the liquid to move within the capillaries. Changes in the back pressure of the entrapped gas will ensure that for any value of applied voltage, the columns of liquid will reach equilibrium positions. The liquid–gas interface may be observed under an optical microscope and recorded with a high-speed camera.

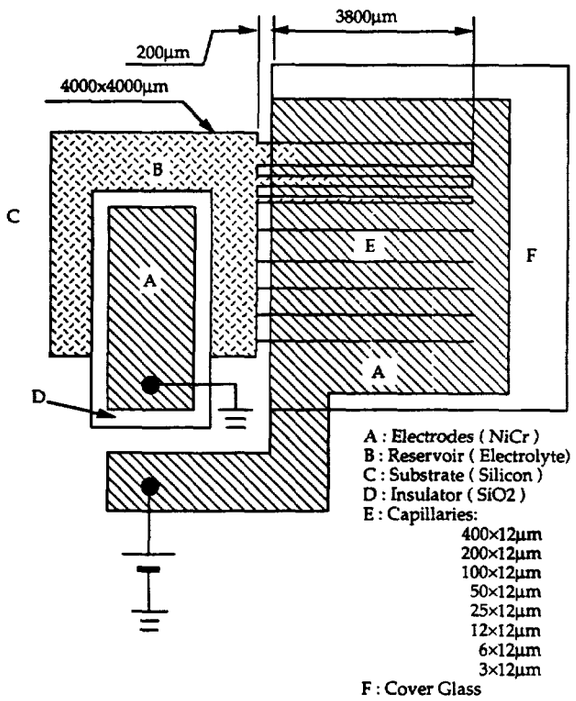

FIG. 3. Schematic of the electrowetting test device.

B. Modeling and simulation

Figure 4 illustrates a single channel. For the purposes of modeling, it will be assumed that the capillaries are circular with radius a; experimental results will be interpreted in terms of the hydraulic radii of the rectangular capillaries. When the fluid is initially introduced to the closed-end capillary, it will be drawn in until the pressure in the entrapped air minus the pressure drop across the liquid–air interface equals atmospheric pressure (because of the size of the device, gravitational effects are negligible):

$$P_G^0 = \frac{2(\gamma_{SG} - \gamma_{SL}^0)}{a} + P_{atm}, \tag{7}$$

where the superscript 0 indicates the initial state. Assuming that the temperature of the entrapped gas reaches atmospheric at equilibrium (a reasonable assumption, because silicon is a good heat conductor), the distance of the interface from the open end of the capillary, ζ^0, can be found from Boyle's Law:

$$\zeta^0 = \left\{1 - \left[1 + \frac{2(\gamma_{SG} - \gamma_{SL}^0)}{P_{atm} a}\right]^{-1}\right\} L. \tag{8}$$

From this initial equilibrium, when a voltage is applied, γ_{SL} will change according to Eq. (6), and motion will ensue. The remainder of this section is devoted to the analysis and simulation of this motion; this analysis will include the following.

(i) The pressure gradient ($-G$) driving the liquid will be determined as a function of V, a, and ζ;

(ii) the centerline velocity v_{max} will be determined on the basis of G and a, assuming steady (Hagen–Poiseuille) flow;

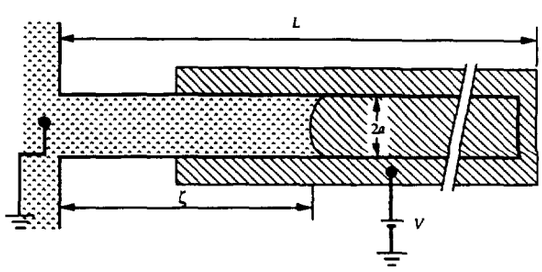

FIG. 4. Schematic of the single channel of the test device.

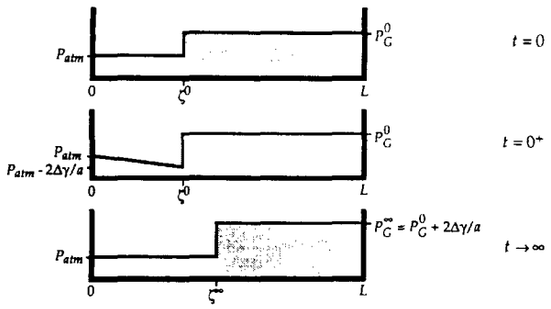

FIG. 5. Three views of the pressure distribution in the capillary. At time $t = 0$, the pressure in the liquid is uniform at P_{atm}, and the interface sustains a pressure drop of $2(\gamma_{SG} - \gamma_{SL}^0)/a$. At time $t = 0^+$, the voltage has been increased from zero, and the pressure drop across the interface increases by an amount $2\Delta\gamma/a$; a pressure gradient is established in the fluid, causing it to move. The fluid continues to move until the pressure gradient drops to zero; in final equilibrium, the pressure in the fluid is again uniform at P_{atm}, and the pressure in the gas has increased by $2\Delta\gamma/a$. Because state changes in the gas are isothermal, the areas of the shaded regions are equal.

(iii) the effect of unsteady behavior on v_{max} will be evaluated.

The result of applying a voltage V will be a reduction in the solid–liquid interfacial tension as follows:

$$\Delta\gamma_{SL} = \frac{\epsilon_r \epsilon_0}{2\delta}(V^2 - 2VV^{zc}). \tag{9}$$

Note that an increase in $\Delta\gamma_{SL}$ will result in a decrease in the interfacial tension; this sign convention has been chosen because any increase in V beyond $2V^{zc}$, as would be typical, will decrease γ_{SL}. The important consequence of a change in V will be a change in the pressure drop across the liquid–gas interface from $\Delta P_0 = 2(\gamma_{SG} - \gamma_{SL}^0)/a$ to $\Delta P_0 = 2(\gamma_{SG} - \gamma_{SL}^0 + \Delta\gamma)/a$ (see Fig. 5). This, in turn, will establish a pressure gradient of $-2\Delta\gamma/a\zeta^0$ over the liquid, which will initiate flow. As the liquid flows, the magnitude of the pressure gradient will decrease due to two physical effects: one, the back pressure increasing as the entrapped gas is compressed; two, the length of the liquid slug, ζ, increasing. Flow will continue until the pressure gradient drops to zero, as illustrated in Fig. 5. A plot of ζ^∞, the equilibrium position of the interface, versus V is shown in Fig. 6 for several values of a.

The (negative) pressure gradient at an arbitrary point in time may be expressed as:

$$G(t) = \frac{dP}{d\zeta} = \frac{2\Delta\gamma/a + P_G^0 - P_G(t)}{\zeta(t)}. \tag{10}$$

If $P_G(t)$ can be expressed in terms of $\zeta(t)$, then the liquid velocity can be determined as a function of interface position. State changes in the gas will be approximated as isothermal because the time constant for heat conduction from the gas to the walls is on the order of $\tau_{cond} = a^2/\alpha$ (α is the thermal diffusivity of air, 2.2×10^{-5} m^2/s at 300 K), which, for the geometries considered here, is short (~ 1 μs) compared to the total movement time (~ 1 ms). The product of gas pressure and $L - \zeta$ is, therefore, constant, and G may be rewritten as:

$$G = \left[\frac{2\Delta\gamma}{a} + \frac{\zeta^0 - \zeta}{L - \zeta} P_G^0\right]\zeta^{-1}, \tag{11}$$

where ζ is understood to be a function of time. Equation (11) is plotted in Fig. 7 for several values of a.

With an expression for the pressure gradient available, it should be possible to solve for v_{max} by applying the Navier–Stokes equations. In the case of steady, laminar flow, the Hagen–Poiseuille solution will suffice:

$$v_{max} = v(r = 0) = \frac{Ga^2}{4\mu}, \tag{12}$$

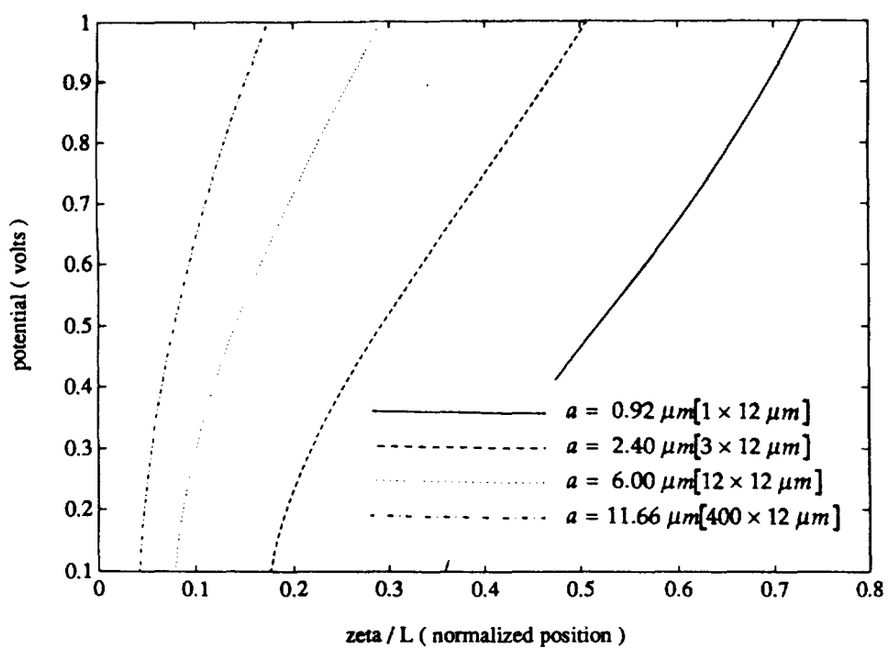

FIG. 6. Interface equilibrium position (ζ^∞) as a function of applied voltage, V. The potential of zero charge is assumed to be zero.

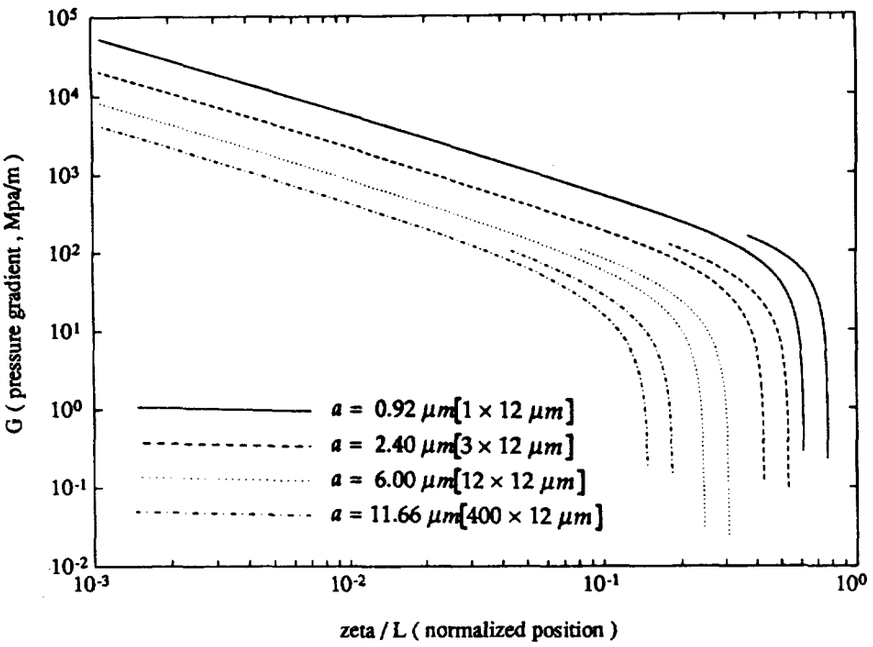

FIG. 7. Negative pressure gradient G as a function of normalized interface position (ζ/L). Two sets of curves are shown; the longer curves are calculated for $\zeta^0 = 0$; the shorter curves are calculated for ζ^0 as given by Eq. (8). The long curves are shown to emphasize that, in the absence of significant back pressure, G varies inversely with ζ, accounting for the straight region of slope $= -1$, and inversely with a. The steep "knee" is due to increasing back pressure in the gas. The short curves correspond to behavior that is expected of the test device. Values used are: $\Delta\gamma = 0.1$ N/m; $\mu = 10^{-3}$ Ns/m^2.

The assumptions underlying the validity of the Hagen–Poiseuille solution, and even of the applicability of the Navier–Stokes equations, however, require careful consideration. These assumptions are as follows.

(1) The flow is laminar. This is a safe assumption: typical Reynolds numbers are 0.1–1.0.

(2) The Navier–Stokes equations apply to flow in microchannels. This is a more tenuous assumption. For instance, for macroscopic laminar flow it is found that the friction factor f relates to the Reynolds number as:

$$f = \frac{C}{\mathrm{Re}},$$

where C is a constant that depends on channel cross-sectional shape, but typically has a value of about 60. Recent experiments, however, have indicated that in microchannels, C may take on values as much as an order of magnitude greater.[9] The experiments to date, however, are inconclusive, and it would be premature to suggest any specific departure from Navier–Stokes. For this analysis, therefore, it will be assumed that the flow is governed by Navier–Stokes.

(3) Reservoir flow is negligible. Because the reservoir is not covered, and is wide compared to the channels, it will offer negligible resistance to flow.

(4) Entrance effects are negligible. Again assuming that the Navier–Stokes equations apply, the entrance length for laminar flow is approximately $L_e = 0.06 D_h \mathrm{Re}$, where D_h is the hydraulic diameter. For the cases considered here, $L_e \approx 0.01$ μm, which can certainly be disregarded.

(5) The frictional effect of the interface region is negligible. This is the least tenable assumption, as it is well-known that capillary flow requires that a finite pressure be applied before movement begins.[10] However, it is found empirically that a frictional surface tension parameter, γ_f, can be defined as:[11]

$$\gamma_f = aP_f/2,$$

where P_f is the minimum pressure required to initiate movement. This parameter can then be used to establish an effective pressure gradient as follows:

$$G = \left[\frac{2(\Delta\gamma - \gamma_f)}{a} + \frac{\zeta^0 - \zeta}{L - \zeta} P_G^0\right]\zeta^{-1}, \quad \Delta\gamma > \gamma_f. \tag{13}$$

This approach assumes that static and kinetic frictional parameters are the same, which is perhaps incorrect; however, neither the current literature nor our own experience offers an acceptable alternative.

(6) Unsteady flow effects are negligible. The unsteady flow solution is discussed below. It is shown that, for the cases considered here, the slowest time constant associated with unsteady flow is $\tau_{\mathrm{unsteady}} \approx a^2/5.76\nu \approx 1$–$23$ μs, which is small compared to the typical duration of movement (5 ms). Based upon these assumptions, $v_{\max}$ was calculated for a constant value of $\Delta\gamma - \gamma_f$ and several values of a. The results are displayed in Fig. 8. Figure 9 illustrates how the interface moves as a function of time.

If the same assumptions as above are made, but the flow is treated as unsteady, then an analytical solution is available in the case of constant pressure gradient, G. This result provides the foundation for a simple numerical solution in the case of time-varying G. The analytical solution can be found by writing the Navier–Stokes equations in cylindrical coordinates and separating variables. The variables are radial position and time; the former leads to a solution in terms of Bessel functions, the latter to an exponential solution. Put together and evaluated on the centerline, the unsteady solu-

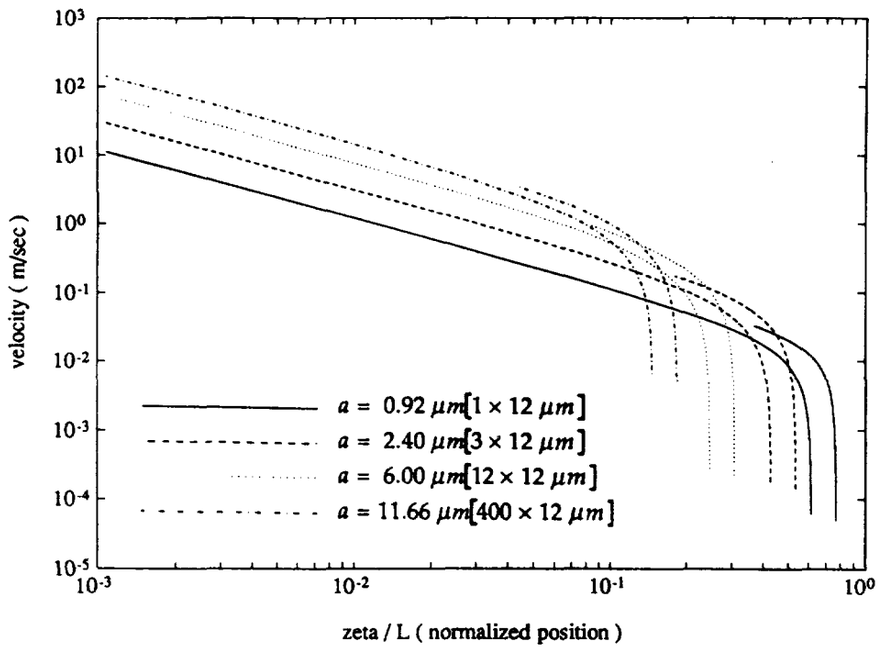

FIG. 8. Centerline velocity (v_{max}) as a function of normalized interface position (ζ/L). Two sets of curves are shown; the longer curves are calculated for $\zeta^0 = 0$; the shorter curves are calculated for ζ^0 as given by Eq. (8). The long curves are shown to emphasize that, in the absence of significant back pressure, v_{max} varies inversely with ζ, accounting for the straight region of slope $= -1$, and proportionately with a. The steep knee is due to increasing back pressure in the gas. The short curves correspond to behavior that is expected of the test device. Values used are: $\Delta\gamma = 0.1$ N/m; $\mu = 10^{-3}$ Ns/m^2.

tion is

$$v_{max} = v(r=0,t) = \frac{Ga^2}{4\mu} - \frac{2Ga^2}{\mu}\sum_{n=1}^{\infty}\frac{1}{\lambda_n^3 J_1(\lambda_n)} \times \exp\left(-\lambda_n^2\frac{\nu t}{a^2}\right), \quad (14)$$

where J_1 is the Bessel function of order 1, and λ_n are the roots of the Bessel function of order 0. The slowest time constant associated with the unsteady solution is evidently $\tau_{unsteady} = a^2/\lambda_1^2\nu = a^2/5.76\nu$. As indicated above, this is typically on the order of 10 μs or less for water in a capillary with radius of 10 μm or less, rendering unsteady effects negligible. The strong dependence upon a, however, as well as the dependence upon kinematic viscosity, suggest that for some systems, which may still be considered micro, the effects of unsteady flow may be significant. An example is the mercury-based micropump proposed in Sec. IV.

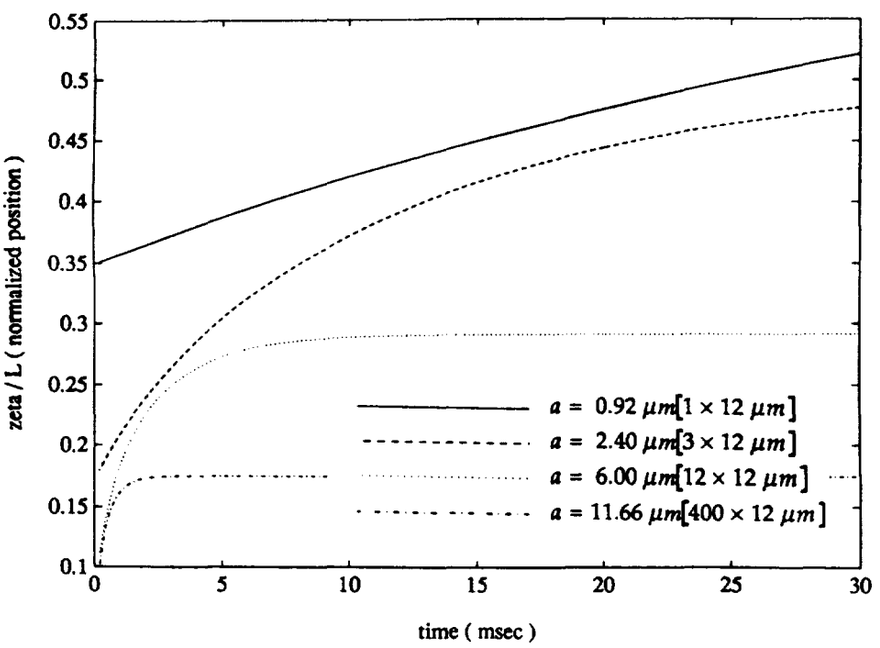

FIG. 9. Interface position (ζ) vs time. Each plot begins at the value of ζ^0 appropriate to its value of a. For smaller radii, the frictional effects become more prominent and the response slows considerably; however, the total excursion increases as the radius decreases.

IV. DISCUSSION

A. Comparison to other microactuators

The basic idea that has been presented here is microactuation based on electrowetting—the electrical control of solid–liquid interfacial tension. The pressure produced by electrowetting is $2\Delta\gamma/a$, which for typical values of $\Delta\gamma$(0.1 N/m) and radii of about 10 μm, is in the range of 0.01 MPa. This is approximately the same pressure as generated by piezoelectric micropumps, which are much larger.

Perhaps a better picture of electrowetting's capabilities can be formed by comparing to other microactuators of similar dimension. A majority of the work on microactuators to date has focused on electrostatic motors, generally of the variable capacitance type. In some designs,[12,13] the plates of the capacitor slide past one another, normal to the field lines, much like the "plates" of the double layer in an electrowetting device. Because of the geometric similarity, comparison is straightforward. It is easily shown that such an electrostatic actuator will produce a lateral force of:

$$F=\frac{\epsilon_r\epsilon_0 l}{2d}V^2, \tag{15}$$

where d is the (fixed) gap between the plates, and l is the width of the plates normal to the direction of movement. If the motor is imagined rolled into a small circle of radius $a=l/2\pi$, it will produce a force per unit area (i.e., pressure or normal stress) of:

$$\Delta P=\frac{\epsilon_r\epsilon_0}{ad}V^2. \tag{16}$$

Assuming typical values of $V=100$ V, $d=1$ μm, $\epsilon_r=1$ (air gap), $\Delta P=2(0.044\ \text{N/m})/a$. The factor 0.044 N/m can be compared to typical values of $\Delta\gamma$, and it is found to be of the same order.

In another design of a variable capacitance electrostatic motor, the plates of the capacitor move toward one another, parallel to the field lines. Such a motor produces a force of:

$$F=\frac{\epsilon_r\epsilon_0 A}{2d^2}V^2, \tag{17}$$

where A is the area of one plate, and d is variable. Because A/ld may be quite large, this motor will produce considerably more force. The difficulty, however, is avoiding "clamp down," and achieving reasonably continuous motion. Several recent designs, however, have worked around these difficulties by clever design of rolling motors.[14,16] Until a linear version is developed, comparison to electrowetting will be difficult, but it is likely that the electrostatic device will produce greater normal stresses.

As a final benchmark, mammillian muscle develops maximum stresses of approximately 0.2 MPa—an impressive figure particularly given the integration of sensing and control, as well as the range of achievable velocities.

B. Pump design

When integrated into a fluid microsystem, the primary goal of the micropump may not be to generate high pressures, but may be, for instance, to generate high flow rates or velocities. One of the difficulties that any fluid microsystem must face is that, at small enough dimensions, frictional effects become extremely important, as indicated in the Hagen–Poiseuille relations:

$$v_{\max}=\frac{a^2}{4\mu l}\Delta P,\quad Q=\frac{\pi a^4}{8\mu l}\Delta P. \tag{18}$$

Velocity reduces as the square of channel radius and flow rate as the fourth power. Even when driven by a pressure that increases inversely with radius, the velocity decreases:

$$v_{\max}=\frac{a}{4\mu l}\Delta\gamma. \tag{19}$$

Suppose, for instance, that $\Delta\gamma=0.1$ N/m, $\mu=10^{-3}$ Ns/m^2, and the desired velocity is 1 m/s (as might be appropriate for microchannel cooling). Then it would be necessary that $l/a\approx 25$. This is a rather small aspect ratio for a fluid system, and seemingly indicative of a fundamental limitation of this type of actuation.

It should be emphasized, however, that there is ample room for creative design. Any actuator design is the consequence of one, some basic physical effect such as magnetism or electrowetting; and two, *geometry*. For instance, although all permanent magnet dc motors work on the same principle —$F=il\times B$—the design choices are many—linear or rotary, number of segments, dimensions, flux return path, permanent magnet stator, or permanent magnet rotor (brushless), etc. These may all be considered geometric factors—ancillary to the basic physics, but essential to the engineering. While it is beyond the intent of this paper to suggest specific geometries for electrowetting micropumps, it is important to illustrate one geometric design feature for which these pumps are, in principle, well-suited—concatenation. It is important because one of the major promises of MEMS is what might be called large scale mechanical integration (LSMI). Of course, necessary precursors to LSMI (or even VLSMI) are the development of (very) small-scale mechanical systems, and means of interconnecting these systems (e.g., concatenation). Figure 10 shows two possible approaches to micropump concatenation: parallel (common pressure, flows sum) and series (common flows, pressures sum). In addition to illustrating concatenation, the parallel design shows how different scales (radii) may be exploited in a single system, and the series design shows how a pump could be built without any moving mechanical parts.

Finally, a somewhat similar, but distinct type of micropump, will be introduced. In this design, illustrated in Fig. 11, the moving liquid is mercury. Because mercury is a metal rather than a electrolyte, there will be no double layer set up upon the application of a potential; instead, a substantial current will flow. In order to establish a capacitance, the electrode surfaces within the capillary must be coated with a layer of dielectric, making this truly a variable–capacitance electrostatic pump of the type described above, Suppose that the radius of the capillary is $a=100$ μm, the length of the mercury slug is 1 mm, and at rest, the pressure of the entrapped gas is 0.1 MPa. Also suppose that the entrapped gas is CO_2 or Freon 12, which have low thermal diffusivities of $\alpha\approx 6\times 10^{-8}$ m^2/s at room temperature. The present goal is to show that this design can act as a resonant microsystem of respectably high Q; i.e., with dynamic effects dominated by

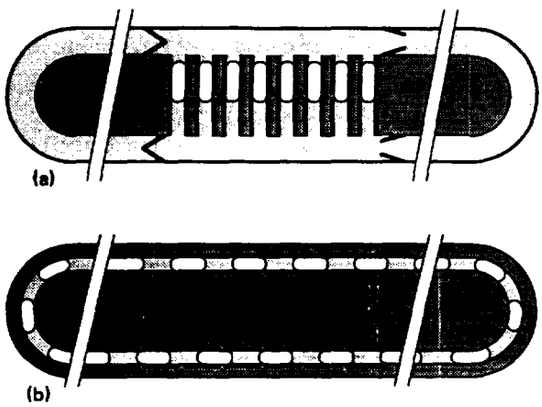

FIG. 10. (a) Common pressure concatenation of electrowetting microactuators. Small black rectangles are electrodes; small radius curves are liquid–gas interfaces. The flow rates produced by the individual electrowetting elements sum to produce the total flow through the system. Notice that the main flow path maybe of a larger diameter, and therefore provide less resistance. (b) Common flow concatenation of electrowetting microactuators. The pressures across the actuated slugs of liquid sum. This is essentially a fluid stepping motor. An appropriate commutation scheme will generate continuous flow; however, the liquid itself cannot be continuous.

kinetic energy storage in the mercury and potential energy storage in the gas, *not* by energy dissipation in fluid friction or heat conduction.

Consider the relevant time constants: for heat conduction, $\tau_{\text{cond}} = a^2/\alpha = 0.17$ s, which is quite slow compared to the period of oscillation (see below), justifying the use of an adiabatic model for the gas; for unsteady behavior the slowest time constant is $\tau_{\text{unsteady}} = a^2/5.78\nu = 0.015$ s, which is still longer than the period of oscillation, thus, a significant portion of the flow is inviscid and inertial effects will be important. A lumped parameter model of the oscillator may be developed as follows: the mass M is that of the mercury slug; the stiffness K is that of the entrapped gas, assuming isentropic state changes, and linearized about the rest position; the friction B can conservatively be estimated as that associated with fully developed, laminar flow:

$$M = \pi a^2 L \rho_{\text{Hg}}, \quad K = \frac{\pi a^2 P_0 \kappa}{l_0}, \quad B = 8\pi \mu_{Hg} L, \tag{20}$$

where L is the length of the mercury slug, P_0 and l_0 are the rest pressure and length of the gas section, and κ is the polytropic index of the gas. From these expressions and the selected parameter values, a natural frequency and damping ratio can be found:

$$\omega_n = \left(\frac{P_0 \kappa}{l_0 L \rho_{\text{Hg}}}\right)^{1/2} \approx 3200 \text{ rad/s},$$

$$\zeta = \frac{4\mu_{\text{Hg}}}{a^2}\left(\frac{l_0 L}{P_0 \kappa \rho_{\text{Hg}}}\right)^{1/2} \approx 0.01. \tag{21}$$

The damping ratio corresponds to a quality factor of 50. This oscillator, therefore, is relatively unaware of fluid dissipation, and may form the basis of an energy-efficient resonant micropump, probably best suited to pumping of low-impedance loads, such as gases.

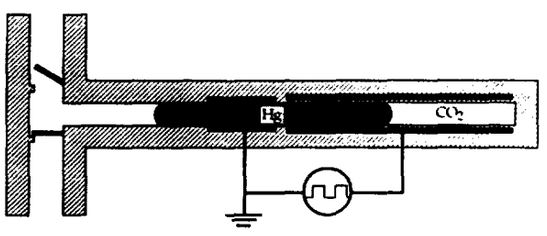

FIG. 11. A variable capacitance micropump. The slug of mercury contacts the ground electrode, and is separated from the drive electrode by a thin layer of dielectric. A voltage applied to the drive electrode forces the mercury slug to the right, compressing the CO_2 gas. A periodic drive signal produces a pumping action.

V. CONCLUSIONS

The feasibility of micropumping based on electrowetting has been considered. A device for testing the electrowetting phenomenon, which is currently under construction, was analyzed in detail. Electrowetting appears to be a viable approach to micropumping, producing pressures comparable to those of existing micropumps, but doing so in a much more compact package (direct fluid pumping is even a possibility). Although the dynamics of the test device are dominated by fluid friction, it was also shown that another micropump design, based on mercury, should behave as a nearly frictionless oscillator. Future research will focus on the realization of both types of micropumps, as well as the concatenation of multiple micropumps.

ACKNOWLEDGMENTS

The authors would like to thank Michael Peshkin for his many insightful comments. H. M. has been supported by NOK Corporation and Nippon Mektron Co., Ltd.

APPENDIX: NOMENCLATURE

a	capillary radius
A	area
B	magnetic field, damping coefficient
C	capacitance
d	capacitor gap width
D_h	hydraulic diameter
f	friction factor
F	force
G	negative pressure gradient
i	current
K	stiffness
l	length or width
L	length of capillary
L_e	entrance length
M	mass
P	pressure
Q	flow rate
r	capillary radial coordinate
Re	Reynolds number
t	time
U	energy
$v_{\max}$	centerline liquid velocity

V	voltage
α	thermal diffusivity
γ	surface or interfacial tension
δ	interphase width
ϵ_0	permittivity of free space
ϵ_r	relative permittivity
κ	polytropic index
λ_n	roots of J_0
θ	contact angle
τ_{cond}	time constant for heat conduction
τ_{unsteady}	time constant for unsteady flow
μ	viscosity
ν	kinematic viscosity
ζ	length of liquid column within capillary, damping ratio

[1]D. B. Tuckerman and R. F. W. Pease, IEEE Electron Device Lett. **EDL-2**, 126 (1981).
[2]S. Sasaki and T. Kishimoto, Electron. Lett. **22**, 1332 (1986).
[3]H. T. G. Van Lintel, F. C. M. Van de Pol, and S. Bouwstra, Sensors Actuators **15**, 153 (1988).
[4]M. Esashi, S. Shoji, and A. Nakano, in Proceedings of the IEEE Workshop on Micro Electro Mechanical Systems, 1989 (unpublished), pp. 29–34.
[5]F. M. Fowkes, in *Chemistry and Physics of Interfaces* (American Chemical Society, Washington, DC, 1965).
[6]P. Sennet and J. P. Olivier, in Ref. 5.
[7]G. Beni and M. A. Tenan, J. Appl. Phys. **52**, 6011 (1981).
[8]G. Wallis and D. I. Pomerantz, J. Appl. Phys. **40**, 3946 (1969).
[9]J. Harley *et al.*, in Ref. 4, pp. 25–28.
[10]M. A. Tenan, S. Hackwood, and G. Beni, J. Appl. Phys. **53**, 6687 (1982).
[11]G. D. Yarnold, Proc. Phys. Soc. London **50**, 540 (1938).
[12]Y. C. Tai, L. S. Fan, and R. S. Muller, in Ref. 4, pp. 1–6.
[13]W. C. Tang, T. H. Nguyen, and R. T. Howe, in Ref. 4, pp. 53–59.
[14]H. Fujita and A. Omodaka, in Proceedings of the IEEE Micro Robots and Teleoperators Workshop, 1987 (unpublished).
[15]W. S. N. Trimmer and R. Jebens, in Ref. 4, pp. 13–16.
[16]S. C. Jacobsen *et al.*, in Ref. 4, pp. 17–24.